Geometric Phase Locked in Fine Structure

Bernd Binder[1]

Date: 16.8.2002, minor corrections, 26.8., 29.8.2002, 1.9.2002

Abstract

Berry's phase carries physical information coded as topological and geometrical objects that can be directly verified in measurements. In some cases the situation can be reduced to an irrational phase shift, that can be usually obtained by an iterative process. Take the Berry phase as the geometric object and let the iterative process be a non-linear phase-locked feedback mechanism defined by spin-orbit coupling and precession, a coupling of fast and slow rotating vectors. For spin-orbit coupling the realization is easy and fast generating irrational and rational numbers: generalized fine structure constants. As a result, this paper provides for additional evidence, that the Sommerfeld fine structure constant α carries a Berry phase component $2\pi(1 - 137\alpha)$.

PACS 03.65.Bz, 03.65.Vf, 06.20.Jr, 12.20.-m, 31.30.Jv

Due to a lack of knowledge, physics theories tend to define and postulated 'second level' constructions and abstractions that cannot directly be observed. This can lead to an inflation of redundant parameters and dimensions. It is the success of math to find short-cuts or 'first level' topological and geometrical constructions that can be directly verified and involve fewer dimensions, Berry's phase is a good example. Generally, phase factors or phases representing the 'holonomy' provide for important boundary conditions while reducing the degree of redundancy in variables, including the phase shifts generated by Berry's connection [1]. The non-adiabatic generalization of [2] defines a geometric phase factor for any cyclic evolution of a quantum system, for an introduction see i.e. [3]. This is one of the reasons why phases and gauge theories are not unimportant in quantum mechanics, despite of the central role of amplitude densities. The fine structure coupling in atomic and molecular dimensions is a candidate for a geometric phase shift:

- it involves fast/slow vector couplings,
- on round trips on a curved surface,
- with exact frequency and phase relationships.

If a geometric phase component generates spin precession, it can couple back to the dynamical phase evolution generating an non-linear feedback loop. In the previous paper [4] such a quantum feedback mechanism has been defined including generalized fine structure constants. The resonances of (atomic) clocks usually depend on phase-locked loops. Controlled by external fields, the geometric phase has a passive role, but in a phase-locked feedback loop the geometric phase has a double role: it is generated on the closed path and controls the closed path length and dynamic phase. Consequently, it is very interesting to consider round trips of vector signals additionally constrained by the precession dynamics induced by an emerging geometric phase.

Round trips

Based on phase-locked round trips of vector signals, a non-linear feedback situation controlled by Berry's phase can be modelled that is compatible with any kind of spin-rotation coupling

[1] *email: binder@quanics.com, Weildorferstr.22, 88682 Salem-Neufrach, Germany* ©*2002*

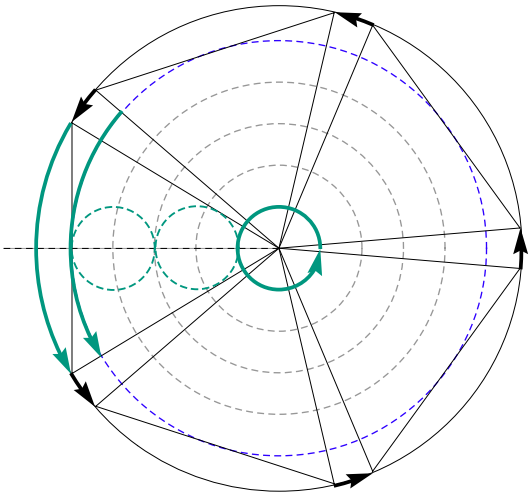

Figure 1: The fine structure M-resonance: all green arrow line segments have the length of the precession cone vertex angle $2\pi\cos(\theta)/M = 2\theta = M_g\triangle\varphi_d(T)$, drawn for $M = 5$ and $M_g = 1$. The two outer circles show the additional contribution of Berry's phase, see the short black arrows with length $\triangle\varphi_g(T)$.

(even gravitomagnetic). Consider round trips of vector signals on spherical paths, where loops induce a geometric phase component. The 'parallel transported' spin vector will come back after every T-periodic loop with a directional change $\varphi_g(T)$ equal to the curvature enclosed by the path $\mathcal{C}$. The Berry phase $\varphi_g(T)$ and the total phase $\varphi(T)$ are proportional to spin J. In the standard case of precession on the sphere

$$\varphi(T) = 2\pi J, \quad \varphi_g(T) = 2\pi J(1-\cos\theta), \quad \varphi_d(T) = 2\pi J\cos\theta, \tag{1}$$

where θ is the vertex cone semiangle and $\varphi_d(T)$ the dynamical phase.
Berry's phase appears if the fast dynamics (spin sub-loops) affects the slow dynamics (orbital loop) and vice versa. A 'rolling cone' representing a vector state or signal is probably the simplest model of spin-orbit coupling. Rotated once, the cone will change its orbital orientation by a special angle $2\pi/M$, rotated M-times in the quantum case, the cone will return to the initial position with integral M (providing for single-valuedness). Visualizing Thomas precession and aberration (angle θ obtained by infinitesimal Lorentz boosts) [5] already pointed out, that the geometric phase can be found in classical mechanics with a gyroscope or point-like compass as a solid-body turn during conical movement [6]. The correspondent cone geometry is shown in fig.2.

Fine structure iteration

The question is, what balances both parts of the total phase? The frequency ratio in a phase-locked situation follows the requirement of single-valuedness and provides for an integral number of M spinning periods on one dynamical phase round trip period (slightly modified by precession). Starting with this model, M can divide the total phase range (slow orbit) into M sub-loop intervals (fast spin) $\triangle\varphi(T) = \triangle\varphi_d(T) + \triangle\varphi_d(T)$ where

$$\varphi_d(T) = M\triangle\varphi_d(T), \quad \varphi_g(T) = M\triangle\varphi_g(T), \quad M = \pm1, \pm2, ... \tag{2}$$

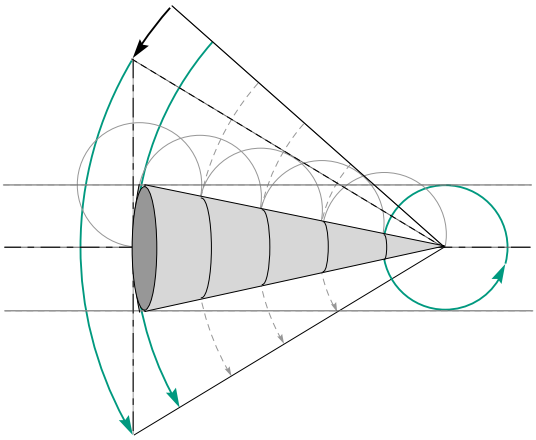

Figure 2: The rolling cone M-resonance: the base of the cone has radius θ/π (small circles), the side length is $M\theta/\pi = \cos(\theta)$. The two green arrow line segments have the length of the precession cone vertex angle and circumference of the cone base $2\pi\cos(\theta)/M = 2\theta = M_g\triangle\varphi_d(T)$, drawn for $M = 5$ and $M_g = 1$. The Berry phase is given by the short black arrow with length $\triangle\varphi_g(T)$.

The effect of precession can be a phase modulation of the orbital path length that could couple to the number of sub-loops by modulating the 'rolling cone path'. Intuitively it should be clear how precession could directly "modulate" the path length and phase on a round trip. In any case it is a non-linear feedback situation where the precession angle will increase with increasing curvature enclosed by the path. The rolling cone resonance, see figs.1 and 2, provides for the feedback relation

$$2\theta = M_g\triangle\varphi_d(T), \tag{3}$$

an orbital resonance condition regarding the dynamical phase and the precession phase. If the cone rotates once, both, the radial and orbital waves will couple back in-phase because of the integral wavenumber on the radial and orbital paths. Now it is possible to find with eq.(1), eq.(2), and eq.(3) the optimum θ for a given M and J, where

$$M\theta = JM_g\pi\cos\theta. \tag{4}$$

As a test for $J = M_g = 1$ and $M > 0$, eq.(4) can be solved by iteration

$$\theta_{i+1} = \frac{\pi\cos\theta_i}{M}. \tag{5}$$

After a few steps the algorithm converges (no problem for $JM_g \ll M$).

Frequencies

Let ω_M be the orbital evolution of the dynamical phase on a circular geometry. The spin-rotation coupling will act on the spinning particle with mass-energy $E = \hbar\omega$ via precession energy $E_p = \bar{\omega}_p$. The relative dynamical coupling strengths can be defined by the ratio

$$\alpha(M) = \frac{J\triangle\varphi_d(T)}{\varphi(T)} = \frac{J\omega_M}{\omega}, \tag{6}$$

a generalized fine structure constant, where the coupling is proportional to the evolution of the dynamical part $\triangle\varphi_d(T)/\varphi(T)$ and to spin J. With eq.(2) in eq.(6)

$$\frac{\varphi_g(T)}{2\pi J} = 1 - \frac{M\alpha}{J}, \tag{7}$$

Table 1:
Convergent fine structure (re)generation constants α for $Z_e = 1$ and variable $M > 2$. The third row shows $N = |\triangle\varphi_d(T)/\triangle\varphi_g(T)|$ or $|N_\pm|$ (bottom), known as winding number on helical paths.

M	J/α	N
3	4.13669	2.63924
4	4.96178	4.15896
5	5.82662	6.04873
6	6.72097	8.32214
7	7.6371	10.98727
137	**137.03600941164**	3804.560912
137	**137.03600998817**	3804.5[1]
137	**137.03600052556**	3805.5[1]
137	**137.03599106791**	3806.5[1]
137	137.03598161523	3807.5[1]

[1] The next hypocycloidal or epicycloidal resonances for $M = 137$ (see fig.4) instead of free running ratio N between dynamical and geometric phase.

the dynamical part of eq.(7) in eq.(1) provides for

$$M\alpha = J\cos(\theta)\,. \tag{8}$$

Comparing eq.(4) with eq.(8) the precession cone vertex angle 2θ of eq.(1) equals the dynamical phase of the spin-orbit interaction part in eq.(2) with

$$\theta = \pi M_g \alpha. \tag{9}$$

The two possible signs can be combined to $M/M_g > 0$

$$M\alpha = J\cos(\pi M_g \alpha)\,, \tag{10}$$

and for $M/M_g < 0$

$$M\alpha = J\cos(\pi - \pi M_g \alpha)\,. \tag{11}$$

Results for α with variable M for $M_g = J = 1$ are shown in table 1, visualized inclusive measurements in fig.3, and simulated with a Java applet in [7].

Topology

As shown by Berry, a geometric phase is produced in the field of a magnetic monopole [1]. Magnetic monopoles are topological in nature and are represented geometrically by non-trivial bundles. For electrodynamics, the gauge group is $U(1)$ which has the topology of a circle, on which the homotopy classes of closed curves are labelled by their winding or loop numbers, and where the magnetic charge is quantized taking integral values [8]. In electromagnetism the charges are multiples of a fundamental charge M, so that the wave-function transforms as

$$\psi \to e^{\pm iM\Lambda}\psi, \tag{12}$$

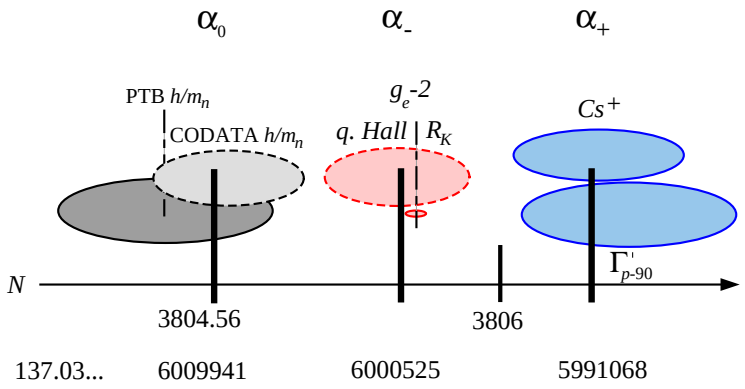

Figure 3: $M = 137$: Regarding the most accurate measurements of the last years there is almost no overlap between the three different setups given by neutron (free running α_0), electronic (epicycloidal α_-), and protonic (hypocycloidal α_+) couplings. Dashed are combined values of different measurements, see [4, 17].

the unit charge corresponds to the phase sub-interval $[0, 2\pi/M]$. The geometrical phase in quantum mechanics is ultimately related to the construction of an Abelian monopole since this is the only topologically non trivial object which arises when the structure group is U(1)[9]. For appropriately chosen base space magnetic monopoles on $SU(2)/U(1) = S^2$, the resulting fiber bundle has a non-trivial topology with non-zero Chern number. It is the total flux produced by the bundle curvature quantized to values $M/2$ with Hopf invariant M and stereographic projection on S^3. The construction of nonsingular vector potentials for a monopole in accordance with Dirac [8], Wu and Yang [10] is shown in fig.4 for $M = 5$. For the two cases of opposite parity (epicycloidal and hypocycloidal) the Berry phase is evolving with or against the dynamic phase. The gradient of the geometric phase (the gauge potential of the monopole) is given by the radial difference in epicycloids-hypocycloid phase evolution. Dirac [8] showed that the existence of magnetic monopoles can explain the quantization of electric charge and that a monopole must carry a magnetic charge which is an integral multiple of 68.5. According to these monopole properties and the U(1) relation to the Berry phase for $J = \frac{1}{2}$, $M = 137$ is the topological candidate to generate the quantum monopole charges of magnetism and electrostatics. Solving eq.(10) or eq.(11) by iteration provides for the balance of dynamical and geometric phase given by α subject to a given number of sub-loops M, coupling loops M_g, sub-loop spin J. The coupling is polar since a positive and negative M/M_g corresponds to the repulsive and attractive case, respectively, in the negative case the coupling phase interval and precession of eq.(9) is negative with respect to the total phase in eq.(2).

Hypocycloidal and Epicycloidal

In addition to the coupling of dynamical phase and conic precession a radial/orbital resonance (single-valuedness) of geometric phase and precession angle could be induced, see fig.4. This situation generates two possibilities: a counter-rotating hypocycloidal system (+) generates more dynamical sub-loops on the total loop than in the co-rotating epicycloidal case (−). Regarding U(1) sub-loops there are two cases characterizing the effects of different sub-loop parity in hypocycloidal and epicycloidal dynamics in terms of coupling constants α_- and α_+, orbital radii R_- and R_+, and rolling radii ρ_- and ρ_+, respectively, for a given small sub-loop radius r_a.

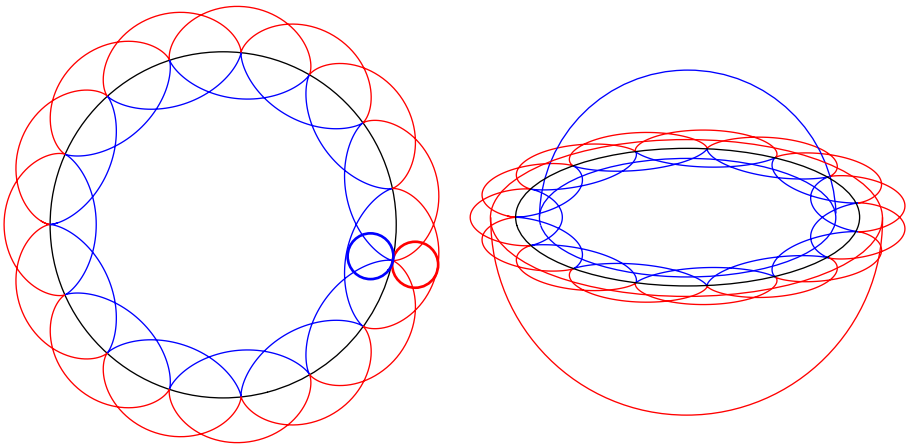

Figure 4: The winding number N-resonance: The spin $\frac{1}{2}$ construction of nonsingular vector potentials for a monopole with charge $M = 5, N_- = N_+ = 7.5$ is given by the connection of epicycloids (outer) and hypocycloids (inner) patches in accordance with Dirac [8], Wu and Yang [10].

Generally

$$R_\pm = N_\pm r_a, \quad \rho_\pm = R_\pm \mp r_a, \quad \alpha_\pm = \frac{J - \frac{J}{N_\pm}}{M}. \tag{13}$$

where the equations for hypocycloidal $(+)$ and epicycloidal $(-)$ paths in the (x, y)-plane with polar angle ϕ are given by

$$\begin{aligned} x &= r_a \left[N_\pm \cos(\phi) \pm \sin(N_\pm \phi)\right] \\ y &= r_a \left[N_\pm \sin(\phi) - \cos(N_\pm \phi)\right]. \end{aligned} \tag{14}$$

The two cases of adjusting epicycloids to hypocycloids (the second case is visualized in fig.4) are given by:

- $N_\pm = N_0$, $R_- = R_+ = R$, the small loops 'roll' at the same radius orbital loop radius but in or on different rings,
- $N_\pm = N_0 \pm 1$, $\rho_- = \rho_+ = \rho$, the small loops 'roll' at different orbital loop radii but in or on the same ring.

The sub-loop rolling or spinning frequency obtained from the 'rolling' velocity $v_\pm$ is given by

$$\omega_\pm R_\pm = v_\pm, \tag{15}$$

where a measurement in the laboratory system is characterized by the invariant ratio

$$\frac{\omega_+ R_+}{\alpha_+} = \frac{\omega_- R_-}{\alpha_-} = c, \tag{16}$$

given by the light velocity $c = v_\pm/\alpha_\pm$. Since $\rho_\pm$ is stationary with respect to the laboratory, comparing $\rho_\pm$ in different cases in terms of N requires no relativistic correction. Consequently, for half spin charges interacting in a hydrogen-type ground state with $N = 3805.5$, the hypocycloidal fine structure constant is decreased in the adjustment (where $N = 3806.5 \to 3805.5$) by $\approx 3805.5^{-2} \approx 6.9 \cdot 10^{-8}$. This shift should appear in fine structure measurements and eventually also in ion mass measurements, since both types shows a different winding number for

the same wavelength and radius. Over the years there was a discussion about the value of the fine structure constant. Different values measured with comparable accuracy disagree in different directions by several standard deviations. The additional quantum condition selecting the hypocycloid or epicycloid character could force extra shifts $\approx N_0^{-2}$, for $M = 137$, see table 1 and fig.3. And indeed, such shifts can be identified by comparing measurements with neutrons, proton or positively charged ions, or electrons [4]. Regarding the α-powers produced with N^2

$$\alpha^2 \approx \frac{2}{\pi^2 N}, \tag{17}$$

the Berry contribution with coupling change $\triangle\alpha/\alpha$ proportional to $1/N^2$ has lowest order α^4-terms. It should be interesting to note, that hyperfine, fine structure, and Lamb shift are usually assigned to the same α-power dependency. It is not clear why geometric phase contributions are missing in almost all perturbative QED evaluations of the atomic spectra.

Hypocycloids and epicycloids can be conformally mapped to other paths. Circles and the tangencies are preserved by the fractional-linear transformations of the Riemann sphere. Entering geometer's world, projective geometry enables to map the epicycloids to hypocycloid and vice versa the signal using conformal transformations, i.e. in the more simpler case by inversions at the sphere combined with translations. In the complex plane Möbius transforms are conformal transformation that always map circles on circles (especially rolling circles!), where a circle is either a usual circle or a straight line, i.e., a circle with infinite radius. In the case of central potentials the transition to polar coordinates and vice versa can be very effectively handled by a conformal mappings involving the complex transformations $\log(z)$ and $\exp(z)$.

Gravitomagnetic coupling

If precession as a frequency ratio is related to a geometric phase

$$\frac{\omega_p}{\gamma\omega} = \frac{\varphi_g(T)}{2\pi J}, \tag{18}$$

and the coupling part to a dynamical phase according to eq.(7) and eq.(6), the general expression for spin-rotation coupling observed in the laboratory frame (relativistic correction γ) can be assumed to be

$$\frac{\omega_p}{\gamma\omega} = 1 - M\frac{\omega_M}{\omega}, \tag{19}$$

or

$$E_p = \gamma(E - M\hbar\omega_M), \tag{20}$$

a generalized form that appears also in gravitomagnetic spin-orbit interaction (Lense-Thirring effect) [11, 12], where an integer M covers scalar and vector fields. Note, that orbital precession of the geometrical phase provides for a change in the frequency ratio

$$\frac{\omega}{M\omega_M} = \frac{1}{\cos\theta} = \frac{\varphi_d(T) + \varphi_g(T)}{\varphi_d(T)}. \tag{21}$$

Usually, the gravitomagnetic effect can be hardly observed because of its tiny magnitude (tests with orbiting gyroscopes are on the way, see gravity probe B news [13]). But the tiny magnitude of the gravitomagnetic field in a classical measurement does not necessarily mean, that the magnitude of the emerging geometric phase and related quantum mass–energy currents in feedback loops must be tiny. Recently, [14] discussed coupling gravitomagnetism-spin and Berry's phase and pointed out, that the geometric phase changes should depend exclusively upon the solid

angle of a field, and not on the strength of the field. In other words, coupling affects the time and length scale but not the phase. In a feedback loop controlled by phase relationships the mass-energy current could increase to a level that is only limited by damping and (multipole) radiation effects, probably a level characterized by electromagnetism. In this nonlinear context it should be mentioned, that with increasing M_g, eq.(10) and eq.(11) characterize a complex one-dimensional system that can show chaotic dynamics and quasiperiodicity [15]. The first bifurcation occur near $M_g = 114$, the next bifurcations occur periodically. Since the production cross section of a super-heavy nucleus was found to be rapidly decreasing with the atomic number near 114 [16], it was concluded that it would be very difficult to reach still heavier elements. For a $J = 1$ vector coupling with charge $Z = JM_g = 114$ chaotic behavior could to some extend be responsible for the instability of the nucleus [4].

Summary and conclusion

The probably most prominent fundamental constant can be within measurement uncertainty reproduced by iterative phase relationships that obey the single-valuedness requirement. Berry's phase can evolve against or with the dynamical phase depending on the sign of curvature (charge). α_0 is based on a plausible connection between the geometric and dynamical phase based on single-valuedness, the winding number enables to construct a magnetic monopole magnetic monopole component to quantize charge, where positive and negative curvatures can be related to the sign in Berry's phase and requires to introduce α_+ and α_- based on the hypocycloidal and epicycloidal character, respectively. Supported by highly rated measurements [17] the epicycloidal $\alpha_- \approx 1/137.03600052556$ with $N_- = 3805.5$ fits within a view ppb to the indirect QED electron $g-2$ determination, the 'free' neutron measurements with $\alpha_0 \approx 1/137.03600941164$ to $N \approx 3804.56$, and the protonic measurements to $N_+ = 3806.5$ with $\alpha_+ \approx 1/137.03599106791$. Additional details can be found in [4].

References

[1] M. V. Berry, Proc. Roy. Soc. Lond. A **392**, 45 (1984).

[2] Y. Aharonov, J. Anandan, 'Phase Change During a Cyclic Quantum Evolution', Phys. Rev. Lett. **58**, 1593 (1987).

[3] R. Batterman, 'Falling Cats, Parallel Parking, and Polarized Light' (2002); PITT-PHIL-SCI00000583.

[4] B. Binder, 'Berry's Phase and Fine Structure' (2002); PITT-PHIL-SCI00000682.

[5] G. B. Malykin, Phys. Usp. **42** (5), 505 (1999).

[6] A. Ishlinski (Mechanics of Special Gyroscopic Systems, Kiev: Izd. AN USSR, 1952).

[7] B. Binder, alpha simulation; http://www.quanics.com/spinorbit.html

[8] P. A. M. Dirac, Proc. Roy. Soc. London A **133**, 60 (1931).

[9] F.V. Gubarev, V.I. Zakharov, Int. J. Mod. Phys. **A17**, 157 (2002); hep-th/0004012.

[10] T. T. Wu, C. N. Yang, Phys. Rev. D, **12**, 3845 (1975).

[11] B. Mashhoon, Gen. Rel. Grav. **31**, 681-691 (1999); gr-qc/9803017.

[12] I. Ciufolini, J. A. Wheeler, "Gravitation and Inertia", Princeton University Press, Princeton, New Jersey, (1995).

[13] Gravity probe B experiment homepage F. Everitt, Stanford.

[14] A. Camacho, 'Coupling gravitomagnetism-spin and Berry's phase'; gr-qc/0206005.

[15] M. J. Feigenbaum, L. P. Kadanoff, S. J. Shenker, Physica D **5**, 370, (1982).

[16] P.H. Heenen, W. Nazarewicz, Europhys. News **33**, No. 1 (2002) http://www.europhysicsnews.com/full/13/article2/article2.html.

[17] P. J. Mohr, B. N. Taylor, Rev. of Mod. Phys., **72**, No. 2, 351 (2000).